

Solar Radio & Geomagnetic Activity Observed in Alaska During August 2022

Whitham D. Reeve

1. Introduction

The month of August 2022 was quite active as recorded by radio and magnetic sensors at the three Alaska observatories: Anchorage Radio Observatory, HAARP Radio Observatory near Gakona and Coho Radio Observatory. The observations included solar radio emissions, meteor trail and aurora radio reflections, sudden frequency deviations and sudden ionospheric disturbances, geomagnetic disturbances and ultralow frequency waves (ULF Waves).

The Sun produced thirty M-class x-ray flares but, surprisingly, no X-class flares (table 1), several coronal mass ejections, almost endless geoeffective coronal hole high-speed streams (CHSS) and accompanying corotating interaction regions (CIR). Most of the strong solar activity took place in the second half of the month. The observations discussed below are a fraction of the total interesting events during August. They span frequencies from mHz to tens of MHz but are not continuous in frequency coverage.

In August 2022, the most active Sunspots and all M-class flares originated from solar Active Regions 3078 and 3088. The activity occurred as Solar Sunspot Cycle 25 ramped up from its beginning in December 2019 (figure 1). It is well known that solar radio emissions and geomagnetic activity increase with the number of sunspots, so the months ahead may prove to be even more active than August.

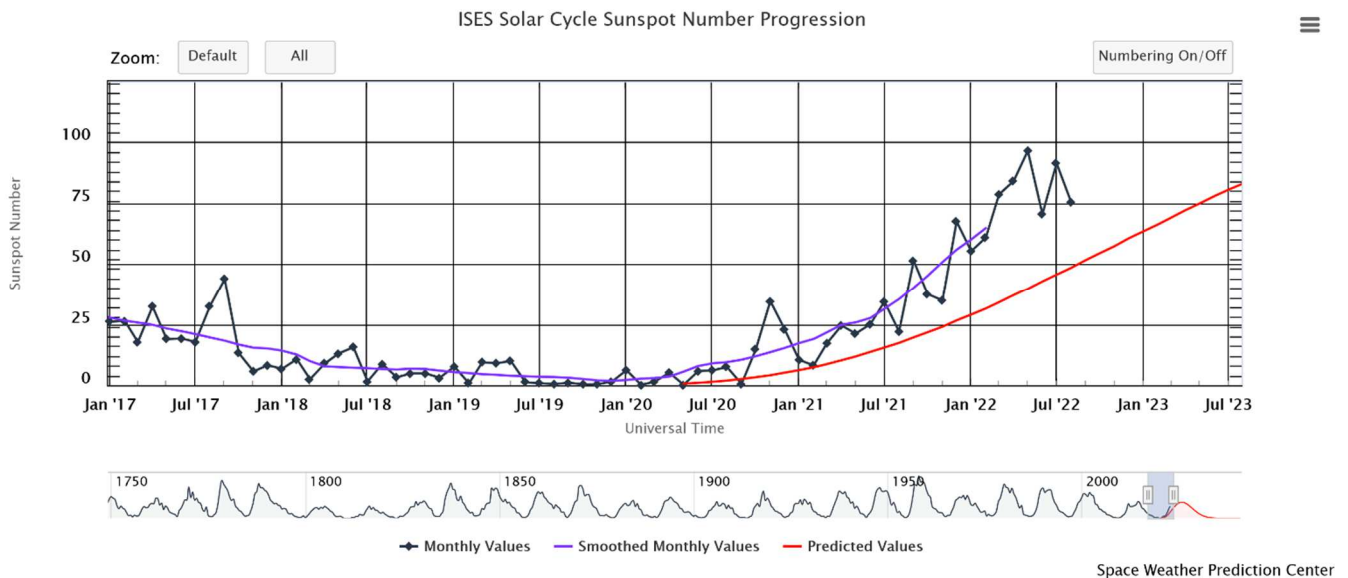


Figure 1 ~ End of Solar Sunspot Cycle 24 and the beginning of Cycle 25 for reference. The lower scale and trace shows the sunspot cycles since 1750; the shaded area on the lower-right shows the range of the upper trace. Image source: [\[SWPC\]](#)

Solar flares often result in radio emissions that are received directly by ground stations on Earth. The high-energy radiation from flares can affect Earth's ionosphere and, thus, terrestrial radio propagation. The radiation effects can be in the form of radio blackouts and sudden frequency deviations (SFD) in the HF band and sudden

ionospheric disturbances (SID) in the LF and VLF bands. Some strong flares produce coronal mass ejections (CME), which in turn can cause Type II slow sweep and Type IV continuum radio emissions from the solar corona and geomagnetic disturbances, the latter delayed by the travel time of the CME from the Sun to Earth. Types of solar radio emissions and their spectral and temporal characteristics are described in detail at [{ReeveSolar}](#).

2. Solar Radio Emissions 5-85 MHz

The first solar radio bursts presented in this section were received on 15 August at HAARP Radio Observatory (figure 2). These Type III sweeps and Type V continuum were received about 2 hours after local sunrise.

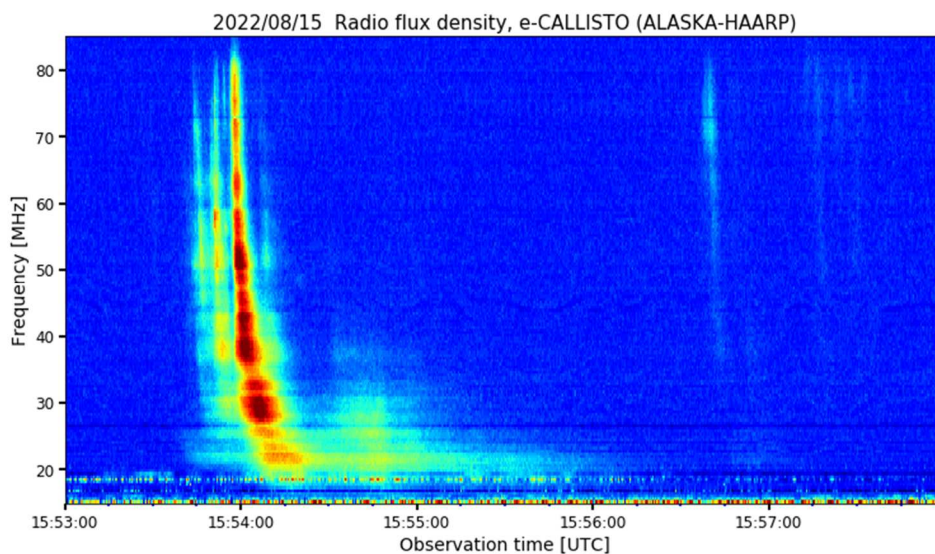


Figure 2 ~ Spectrogram from HAARP shows Type III fast sweep radio bursts received at 1554 on 15 August, which covered the 15-85 MHz frequency range. The sweeps were immediately followed by a Type V continuum between 17 and 39 MHz. Additional weak Type III radio sweeps are seen toward the end of this record. The broken horizontal lines below 20 MHz are terrestrial HF transmissions.

Earth's ionosphere usually is opaque to celestial radio emissions below about 15 MHz, but the actual blocking frequency can occasionally reach as low as 5 MHz. Two of the three Callisto installations in Alaska are set to observe down to 5 MHz as part of a long-term study of the ionosphere's blocking frequency at high latitudes. A consequence of operating at the lower frequency is the ever-present terrestrial HF traffic, a form of unavoidable interference. The traffic is seen as solid or broken horizontal lines on the spectrograms.

The HAARP science facility is multiuse with many diagnostic instruments and other types of instrumentation including a local ionosonde (DigiSonde) and a sweeping transmitter on the TCI-540 HF antenna. This antenna has a low elevation angle and is used for ocean scatter experiments. These systems result in slanted lines below 25 MHz on the HAARP spectrograms. There is very little interference from HF transmissions at Coho Radio Observatory.

Additional solar radio emissions were received at HAARP on 19 August (figure 3). The form of this spectra does not conveniently fit any specific radio burst Type and probably is an overlay of more than one burst type or bursts from more than one solar region received at the same time.

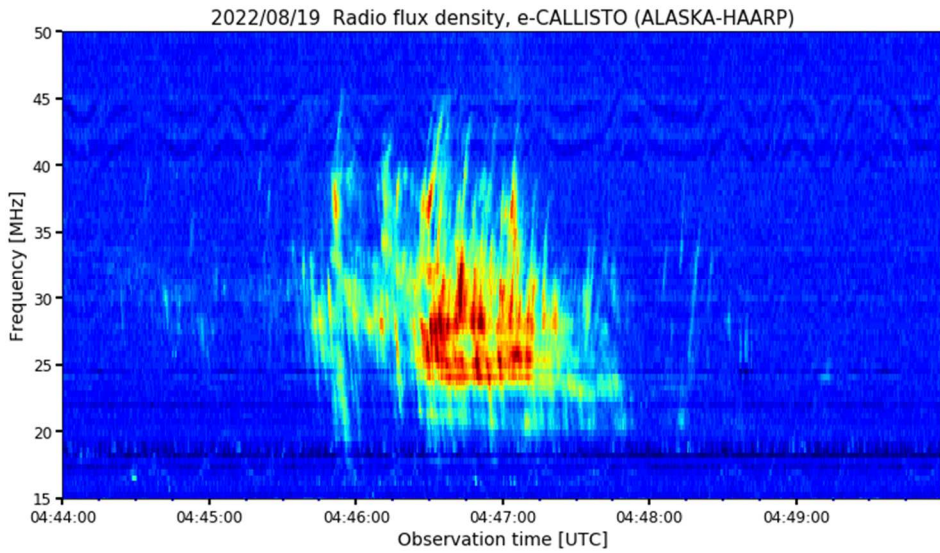


Figure 3 ~ A spectrogram from HAARP on 19 August shows radio emissions associated with an M1.6 x-ray flare that began at 0414, peaked at 0444 and ended 0518. Type II, III, IV and VI sweeps were reported with this flare by Space Weather Prediction Center, but the type shown on this spectrogram is unknown. It could be a combination of Type II and IV or III. Some of the spectra appears to sweep from low to high frequencies, opposite of normal.

Type IV broadband continuum emissions take on several forms, one of which is called Stationary Type IV Broadband Continuum with Fine Structure. It is related to flares and proton emission. Such a radio continuum resulted from an M4.8 x-ray flare and was received at both HAARP and Coho on 27 August (figure 4 and 5). Broadband continuum emissions usually are very weak when received on Earth and the associated spectrograms often show background noise or other system-related spectral defects resulting from the spectrum image processing.

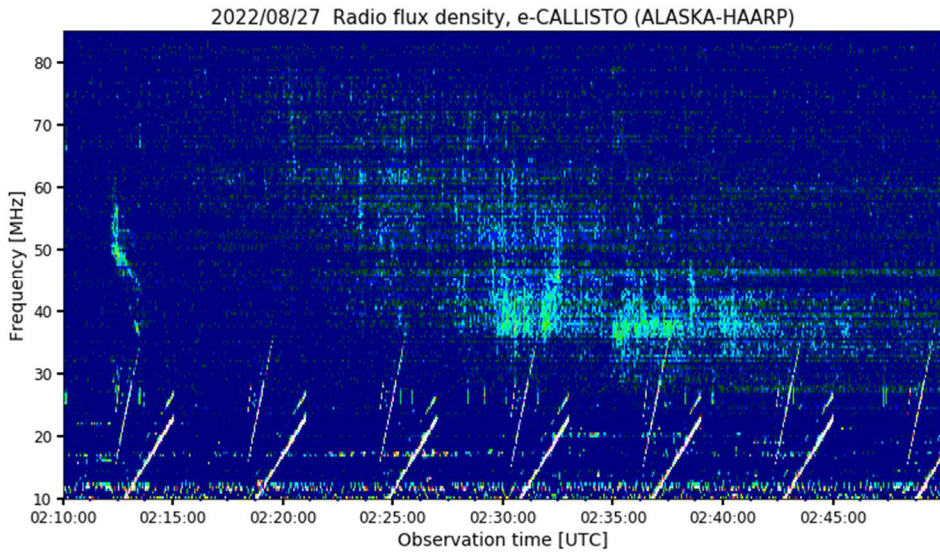


Figure 4 ~ A Type IV broadband continuum was received at HAARP on 27 August. It was associated with an M4.8 x-ray flare that began at 0152, peaked at 0240 and ended 0305. The continuum was very weak so the background was enhanced, which resulted in some horizontal banding in the spectra. The slanted lines are local HF transmissions.

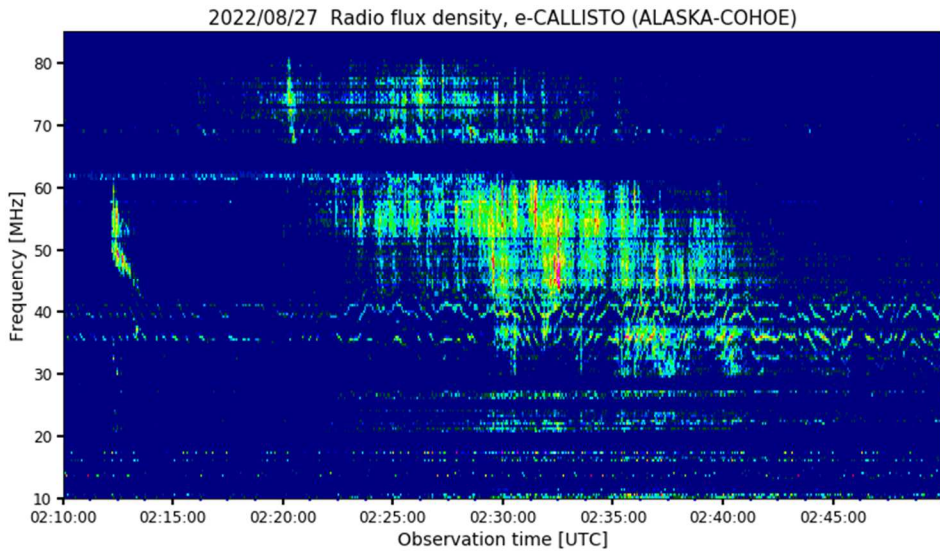


Figure 5 ~ This spectrogram from Cohoe was processed using the same frequency and time settings as the HAARP spectrogram above. The Cohoe spectrogram shows a dropout centered on 65 MHz due to FM broadcast band intermodulation interference. The spectrogram also shows wavy lines between 36 and 40 MHz that may be self-generated interference from system power supplies.

A short-lived continuum with Type II slow radio sweep and other spectral oddities was received at HAARP on 29 August about 2.5 hours after sunrise (figure 6).

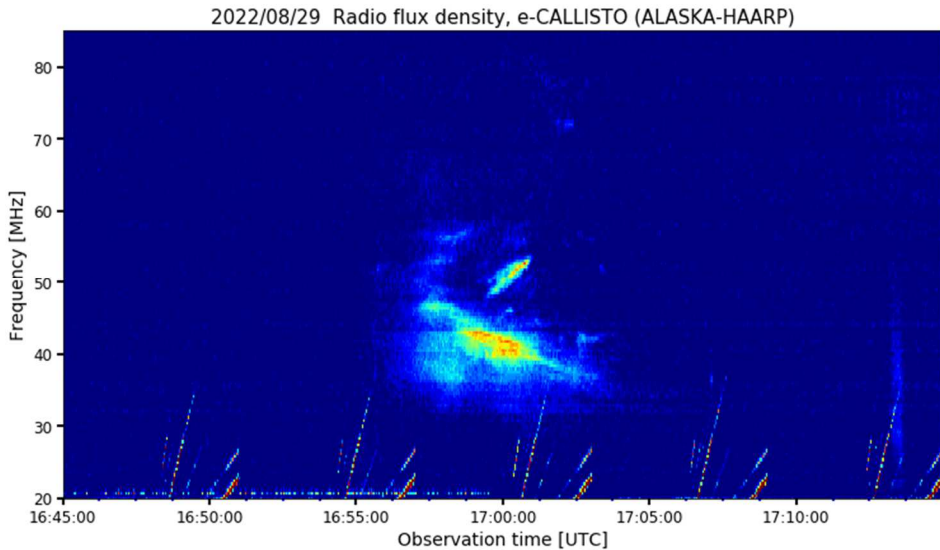


Figure 6 ~ Solar radio burst received at HAARP on 29 August had weak spectral components to at least 85 MHz (the upper limit of the up-converter used with the Callisto instrument). A weak Type III radio sweep appears near the end of this record. The slanted lines are local HF transmissions.

3. Meteor Trail Reflections at 20 MHz

The narrowband Argo spectrogram below (figure 7), dated 16 August, is from Anchorage Radio Observatory and shows meteor trail reflections at 20 MHz from WWV (Colorado) or WWVH (Hawaii). The time frame of the plot corresponds to the Perseids meteor shower, which was active between about 14 and 24 August, but the meteors recorded may very well be random. A basic requirement of receiving meteor trail reflections at Anchorage while using the WWV or WWVH transmitters (both around 4000 km away), is that a multimode propagation path must exist from the distant transmitters to the location of the meteor trail at approximately 100 km altitude and from that location to the receiver. Experience has shown that a path from the transmitter

to the receiver (not reflected) must also exist at the time. The actual location of the reflection region is unknown. Receiving meteor trail reflections at HF is fully described at [{ReeveMeteor}](#).

For display on an Argo plot, the 20 MHz carrier has been demodulated using LSB mode. The receiver was tuned to 20.001 005 MHz, so the carrier corresponds to the 1005 Hz trace on the plot. The trace at 995 Hz is the demodulated WWV or WWVH carrier at 15 MHz. In this case, the receiver was tuned to 15.000 995 MHz, but no meteor trail reflections are seen on it.

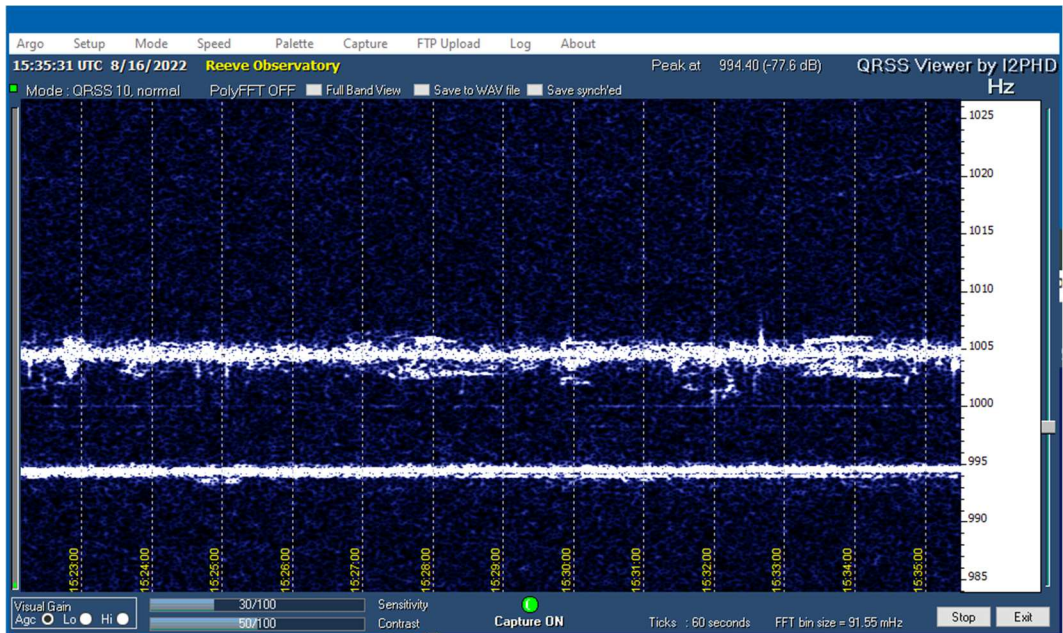


Figure 7 ~ This Argo plot from 16 August shows several short duration (vertical ticks) and a few long duration (horizontal striated lines) meteor trail reflections. The carrier at 20 MHz is represented by the jagged horizontal line at 1005 Hz. The line at 995 Hz represents a carrier at 15 MHz but it shows no reflections.

4. Aurora Radio Reflections at 15 and 20 MHz

The geomagnetic disturbances during August led to aurora activity north of Anchorage Radio Observatory and the reception of radio reflections at 15 and 20 MHz, examples of which are shown (figure 8). The receiver and antenna setup for receiving aurora radio reflections is the same as for meteor trail reflections; however, in this case the transmitter is believed to be WWVH exclusively because of its favorable north-south alignment with Anchorage Radio Observatory.

The presumed aurora reflection regions are believed to be around 500 to 1000 km north of Anchorage, which requires a multimode propagation path from Hawaii to the aurora reflection region at 100 to 120 km altitude and from there back to Anchorage. The received reflections take on many spectral forms, but all include rapid or high Doppler frequency shifts and signal level enhancements. Also, all aurora radio reflections are associated with geomagnetic disturbances, particularly rapid decreases or increases in the magnetic field flux density measured by the Anchorage SAM-III magnetometer. A detailed discussion of aurora radio reflections can be found at [{ReeveAurora}](#).

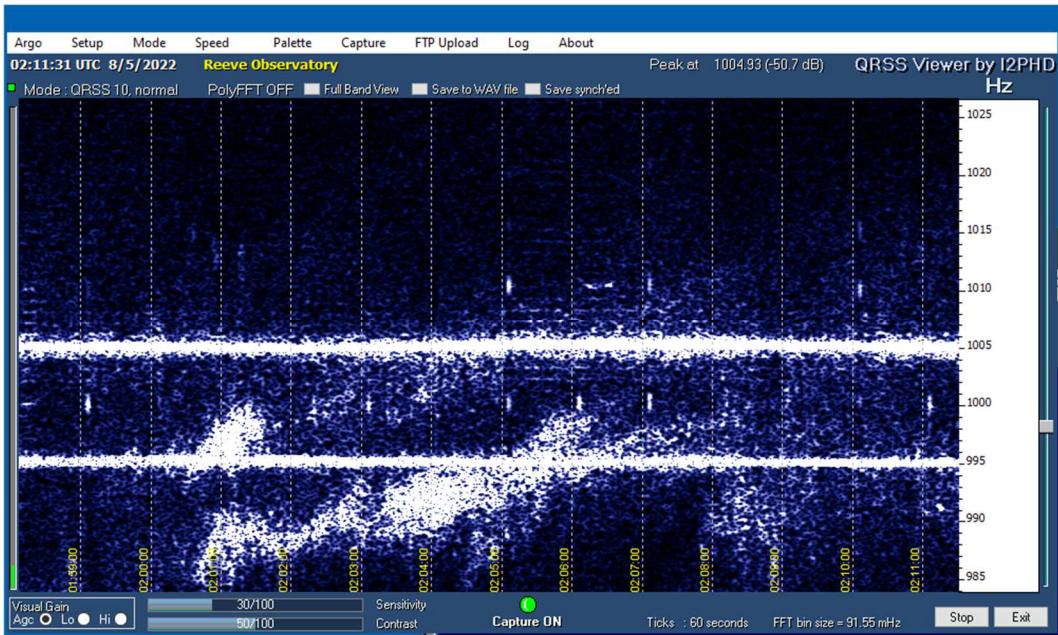


Figure 8.a ~ Aurora radio reflections on 5 August at around 6:00 pm local time (0200 UTC). These reflections are the diffused type with a slanted, blob-like structure. These appear to be at both 15 and 20 MHz (995 and 1005 Hz, respectively, on the right frequency scale). The short, vertical ticks are processing artifacts of the WWVH minute time marks.

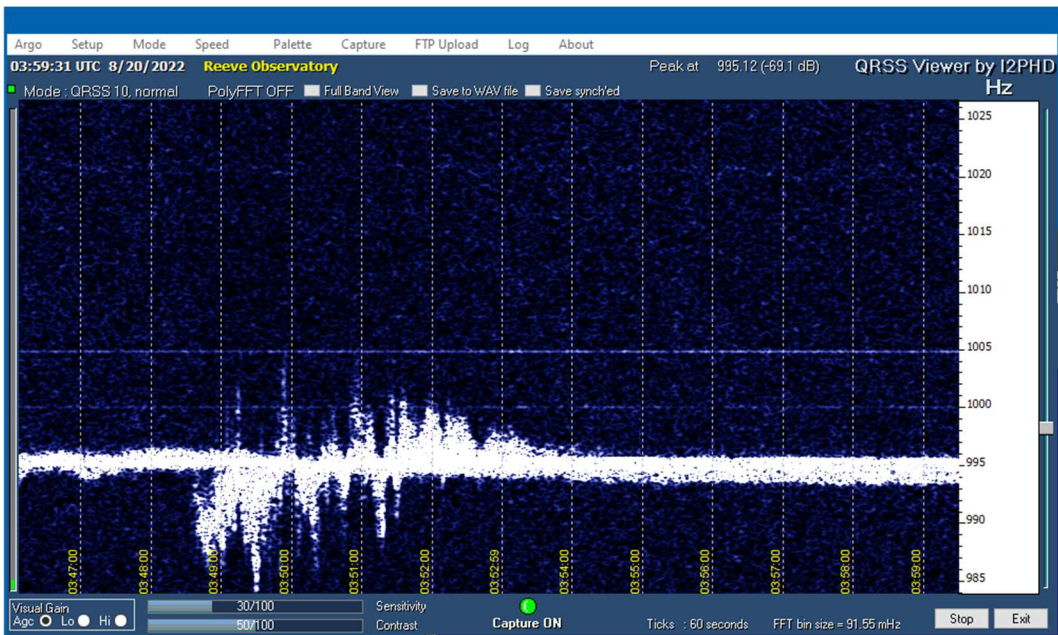


Figure 8.b ~ Aurora radio reflections on 20 August around 8:00 pm on 15 MHz only (995 Hz on frequency scale). No signal is received at 20 MHz (1005 Hz on frequency scale). The Doppler frequency shift is at least -10 Hz to $+6$ Hz.

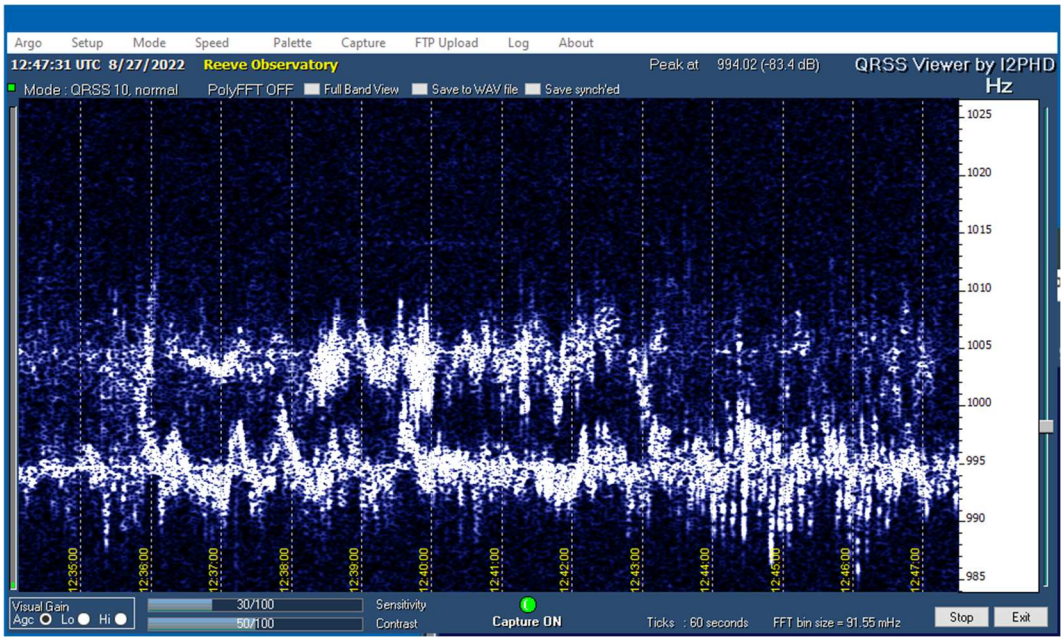


Figure 8.c ~ Early morning aurora radio reflections on 27 August at both 15 MHz (995 Hz on frequency scale) and 20 MHz (1005 Hz on frequency scale). The local time is around 4:40 am (1240 UTC).

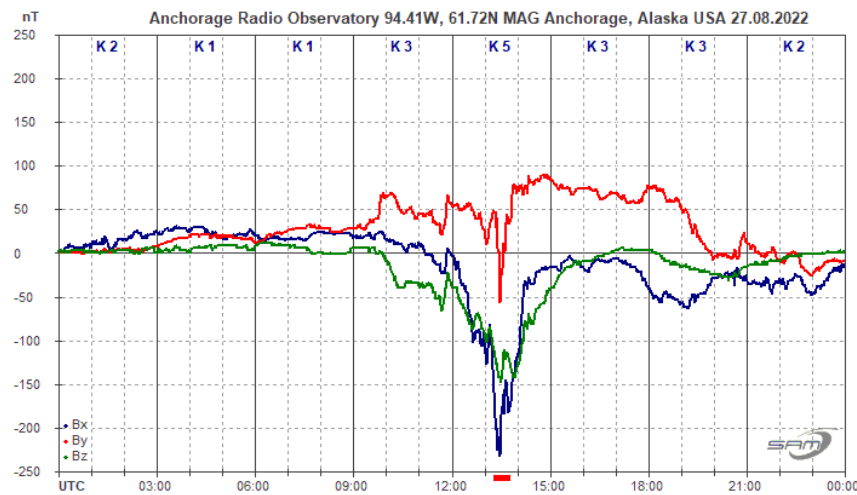


Figure 8.c.1 ~ Geomagnetic activity between 1235 and 1247 corresponds to the aurora radio reflections seen in the previous image. The magnetic bay between 1200 and 1400 is a strong indicator of aurora and their associated magnetic field-aligned enhanced electron density regions where the reflections take place.

5. Sudden Frequency Deviation on 15 and 20 MHz

Sudden frequency deviations, SFD are direct evidence of solar flare radiation affecting Earth's ionosphere by rapidly moving the ionosphere's reflection region (modeled as a slab of electrons), thus altering the propagating signal's wave number and frequency. Two SFDs are shown here on 15 and 16 August (figure 9 and 10, respectively). The radio system setup for observing sudden frequency deviations is identical to that used for meteor trail and aurora radio reflections discussed above. Sudden frequency deviations at HF are fully described at [{ReeveSFD}](#).

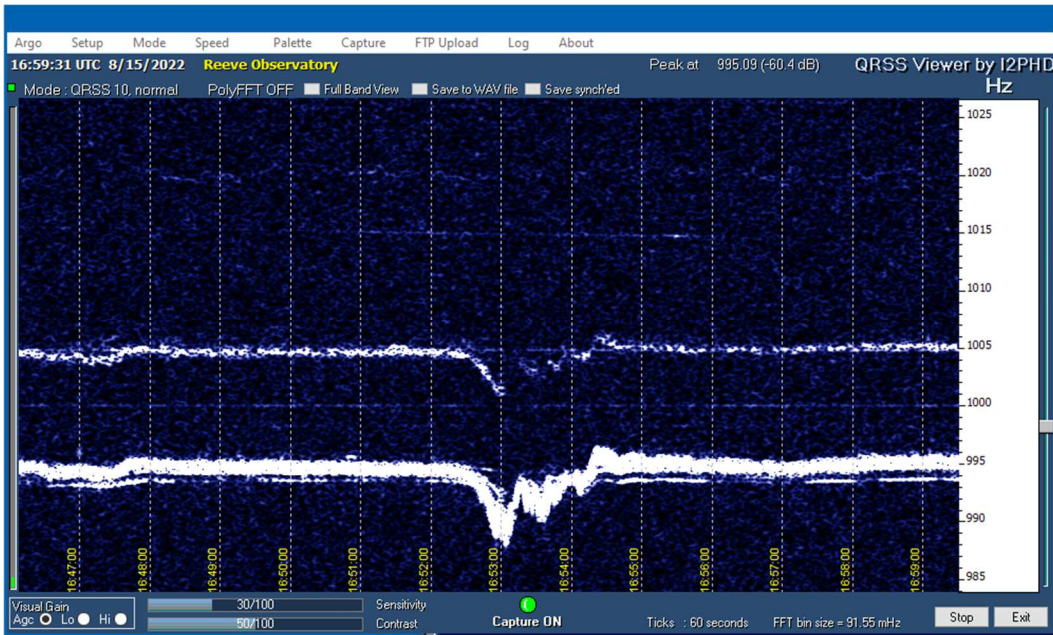


Figure 9 ~ Sudden frequency deviations on 15 and 20 MHz at 1653 UTC on 15 August caused by an M2.7 x-ray flare. Note the small precursor deviation at the beginning of the plot. The transmitted carrier, receiver and displayed frequencies are as described for meteor trail and aurora radio reflections discussed above.

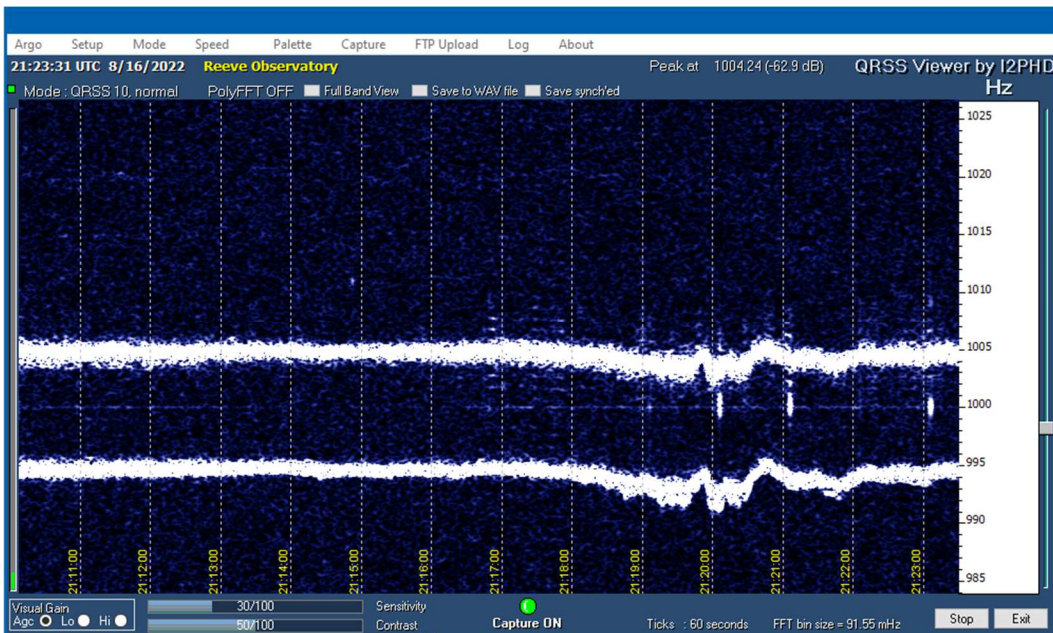


Figure 10 ~ Sudden frequency deviation on 16 August caused by an M1.8 x-ray flare at both 15 and 20 MHz. This SFD started about 2118 with full effects at 2120 UTC. The vertical ticks just below the upper trace are processing artifacts.

6. VLF and LF Sudden Ionospheric Disturbances

Sudden ionospheric disturbances (SID) are like sudden frequency deviations in that solar flare radiation affects the ionosphere in such a way that radio propagation also is affected. In the case of SIDs, it is the transmissions from high power, low frequency transmitters used for submarine communications that are being continuously monitored. In most cases, signal propagation is enhanced so that the received signal level increases during the flare.

During August 2022, Cohoe Radio Observatory had two VLF/LF receiver/loop antenna systems in operation. One recorded the received signal level from station NPM in Hawaii on 21.4 kHz (figure 11) and the other recorded the signal levels from station WWVB in Colorado on 60 kHz (figure 12). NPM is almost due-south of Cohoe with an overwater path length of about 4400 km, while WWVB is almost due-east of Cohoe with an overland path length of about 3800 km.

Both systems occasionally experience severe interference believed to be from nearby powerlines. The interference was more severe at 60 kHz and, along with weaker received signal levels, the plot for WWVB is very ragged.

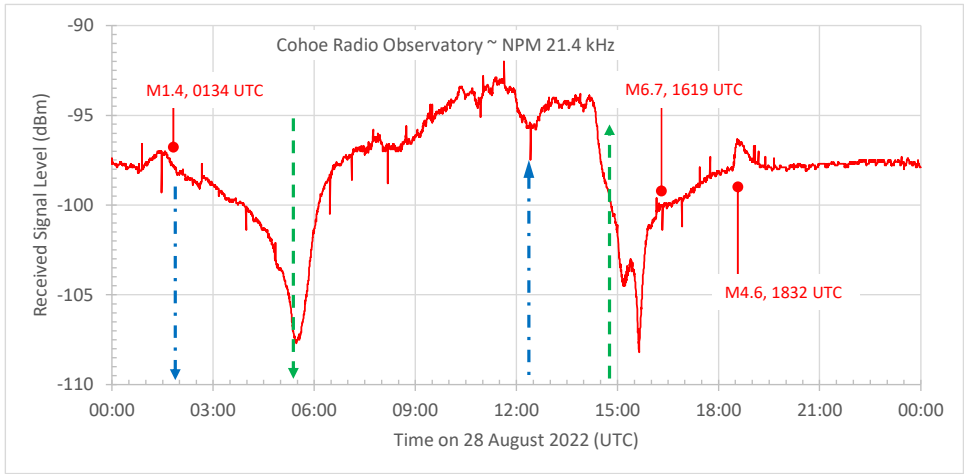


Figure 11 ~ Plot of NPM received signal level for 28 August at Cohoe Radio Observatory. Three M-class x-ray flares occurred during the daylight hours at Cohoe and each left a small imprint on the received signal level. Sunset and sunrise effects are most apparent at the Cohoe end. Sunset and sunrise times are shown by down and up arrows for Cohoe (green dashed) and WWVB (blue dotted-dashed).

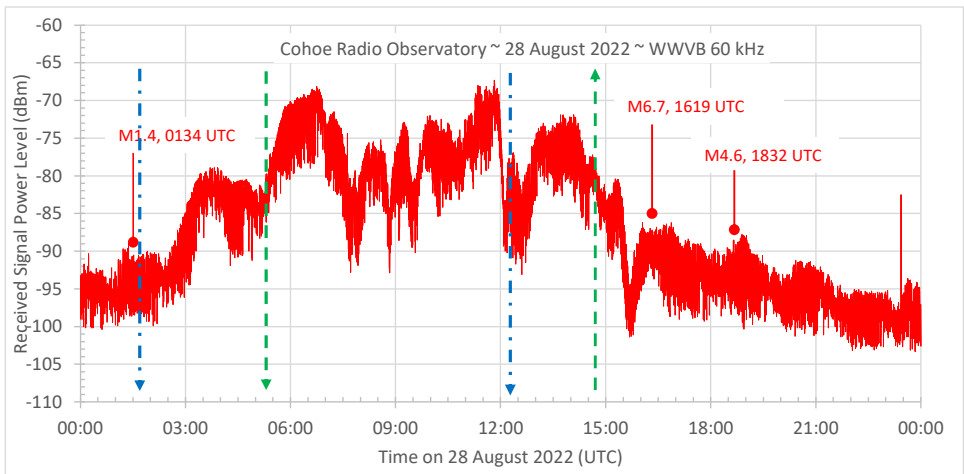


Figure 12 ~ Received signal level on 28 August from WWVB at 60 kHz. The Cohoe sunrise and sunset shown in green dashed lines and WWVB shown in blue dotted-dashed lines. The sunset and sunrise at both WWVB and Cohoe affected the signal received at Cohoe.

7. Geomagnetic disturbances and ULF Waves

Geomagnetic disturbances result from many phenomena in the solar wind, such as coronal hole high-speed streams, coronal mass ejections and merging of Earth's magnetic field with the interplanetary magnetic field (IMF). These disturbances are seen on magnetograms, which were produced by the SAM_VIEW software and the SAM-III magnetometer at Anchorage Radio Observatory. A consequence of many disturbances in the solar wind is the production of ULF Waves in the Earth's magnetospheric cavity. ULF Waves are electromagnetic with

frequencies that range from a few Hz to a few mHz. The magnetic component is detected by ground magnetometers and appear on magnetograms as rapid pulsations with quasi-sinusoidal waveforms. A geomagnetism tutorial may be found at [Geomag](#). ULF Waves will be covered in detail in a future paper and SARA conference presentation.

On 8 August, geomagnetic disturbances from coronal hole high-speed streams led to storm conditions and erratic magnetic field variations throughout the day (figure 13).

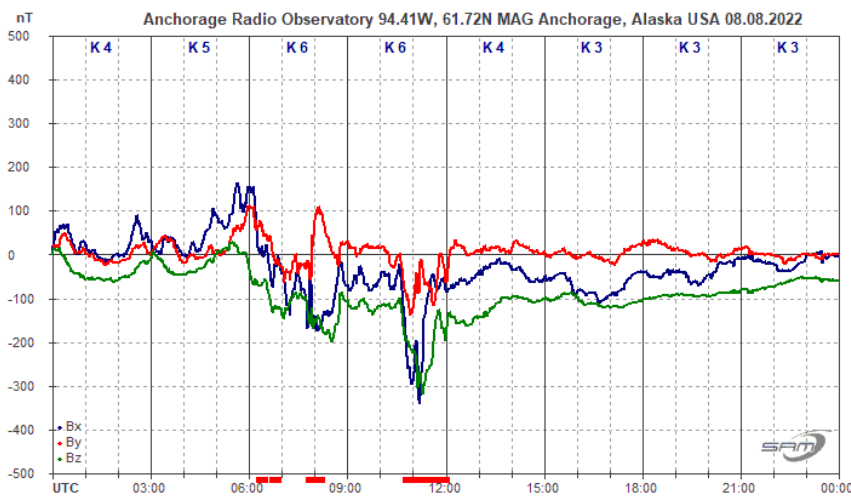


Figure 13 ~ On 8 August, geomagnetic disturbances from coronal hole high-speed streams led to storm conditions with K-index K5 or higher in the 0300-0600, 0600-0900 and 0900-1200 synoptic periods. Earth's magnetic field showed erratic deviations during these periods but quieted down after 1200.

A geomagnetic sudden impulse was observed 17 August at 0303 UTC (figure 14.a). A geomagnetic storm often follows soon after a sudden impulse but, in this case, the storm actually occurred 33 hours later. ULF Waves, which appear as rapid pulsations on a magnetogram, can be seen during at least two periods. The ULF Waves appear quite weak on the 2-day magnetograms because of the relatively high vertical scale needed to display the overall magnetic deviations. Individual magnetograms and a selected plot with smaller vertical scales show more detail (figure 14.b, 14.c and 14.d).

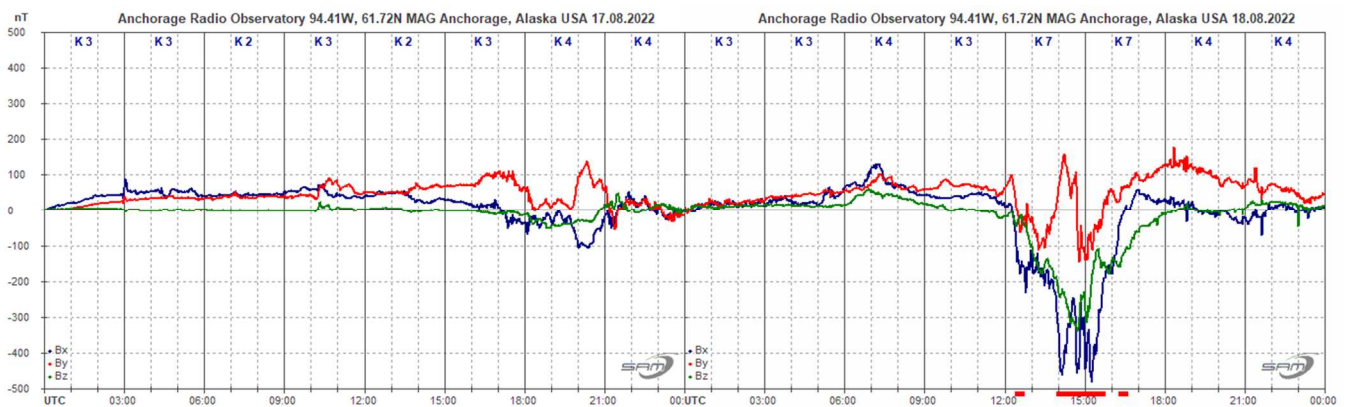


Figure 14.a ~ Two 24 hour magnetograms spliced together to show the sequence of events for 17 and 18 August after a sudden impulse at 0303 UTC on 17 August. The sudden impulse resulted from a coronal mass ejection a few days before. There were relatively mild follow-on geomagnetic disturbances about 14 hours later at 1700 through 2300. ULF Waves also were generated about the same time and appear between 1600 and 1800 and between 2100 and 2400 on 17 August,

continuing until about 0400 the next day. Storm conditions were reached on 18 August during the 1200-1500 and 1500-1800 synoptic periods during which ULF waves also were observed.

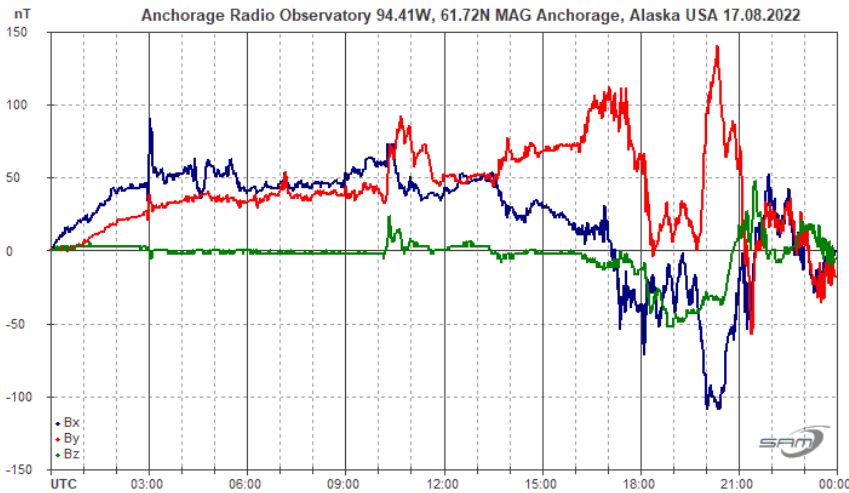


Figure 14.b ~ Magnetogram for 17 August more clearly shows the sudden impulse at 0303 and ULF Waves between approximately 1630 and 1800 and between 2100 and 2400, the latter spilling into the next day as shown below.

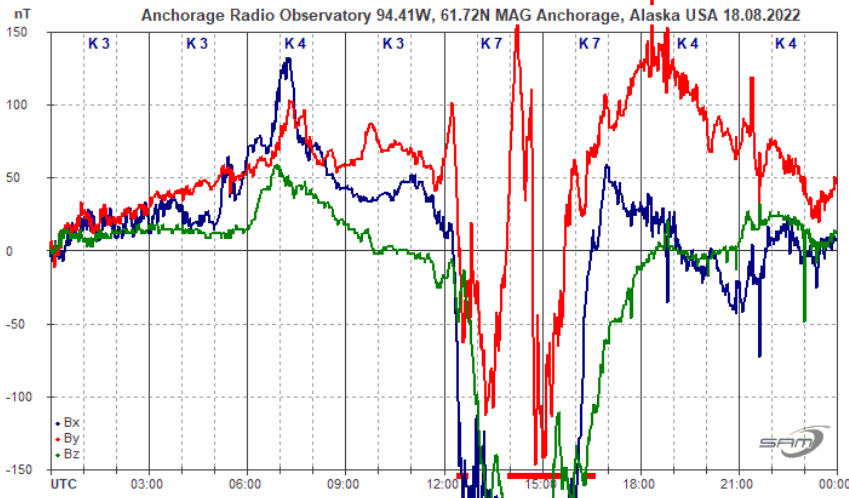


Figure 14.c ~ Magnetogram for 18 August at a fixed scale to show ULF Waves at the beginning of the UTC day from 0000 to about 0500. ULF Waves also are visible between approximately 1700 and 2400 in both the X- and Y-axes.

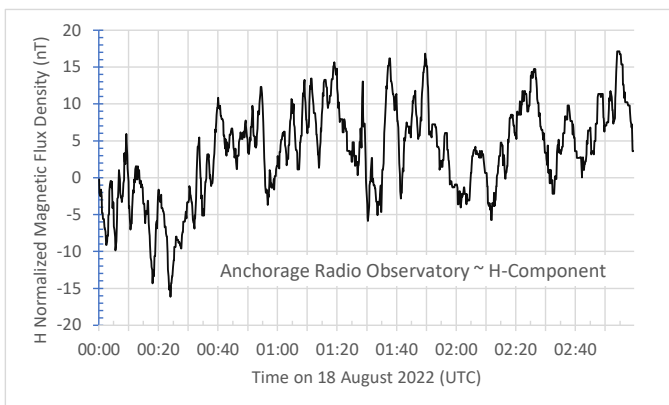


Figure 14.d ~ Normalized plot showing ULF Waves from 0000 to 0300 on 18 August. This plot shows the horizontal, or H, component, which is the vector sum of the X- and Y-axis magnetic flux density from the previous magnetogram. There are 51 cycles in this 3 hour time span, giving an average period of 212 s and an equivalent frequency of 4.7 mHz.

The Bartels Diagram provides a visual summary of geomagnetic activity in terms of a 27 day solar rotation with 3 hour resolution. Bartels Diagrams for the time period 1 August through 4 September 2022 are shown (figure 15).

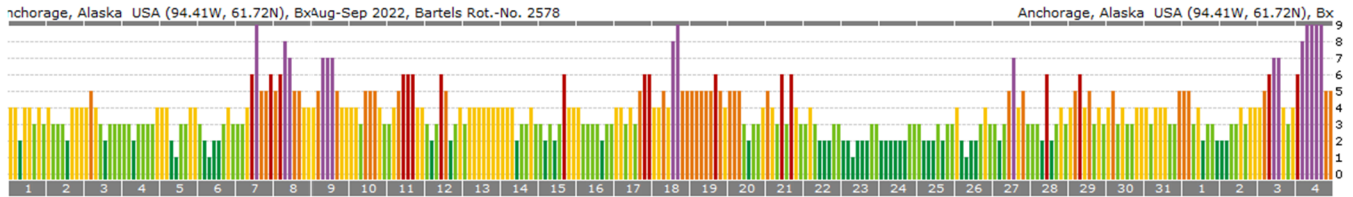


Figure 15 ~ Bartels Diagram for rotations 2577 and 2578 stitched together to show relatively high geomagnetic activity on 7-8 August as well as 27 days later on 3-4 September. The enhanced activity of 18 August coincides with the storm conditions previously described. This plot was produced by SAM_STAT software using the SAM-III data.

Table 1 ~ M-Class Flares during August 2022. Solar transit is within 20 min of 2200 UTC at all observatories. Shading indicates flares that occurred after sunset. Source: Space Weather Prediction Center weekly reports ([Weekly](#))

Flare class	Date (UTC)	Max Time (UTC)	Active region	Daylight	Sunrise/sunset
M1.0	15 Aug	1436	3078	After sunrise	1409/0601
M2.7	15 Aug	1654	3078	After sunrise	
M0.9	15 Aug	1733	3078	After sunrise	
M1.1	15 Aug	2153	3078	Transit	
M5.0	16 Aug	0758	3078	After sunset	1412/0558
M1.8	16 Aug	2121	3078	Transit	
M2.0	17 Aug	1345	3078	Before sunrise	
M1.0	17 Aug	1452	3078	After sunrise	
M1.3	18 Aug	1009	3078	Before sunrise	1417/0552
M1.5	18 Aug	1055	3078	Before sunrise	
M1.3	18 Aug	1413	3078	Before sunrise	
M1.6	19 Aug	0444	3078	Before sunset	1419/0549
M1.8	25 Aug	1951	3078	After sunrise	1435/0530
M1.0	25 Aug	2327	3078	After transit	
M2.1	26 Aug	1055	3078	Before sunrise	1437/0527
M7.2	26 Aug	1214	3078	Before sunrise	
M5.3	26 Aug	1231	3078	Before sunrise	
M4.8	27 Aug	0240	3078	Before sunset	1440/0524
M1.2	27 Aug	1138	3078	Before sunrise	
M1.1	27 Aug	1525	3078	After sunrise	
M1.8	27 Aug	1558	3078	After sunrise	
M1.4	28 Aug	0134	3078	Before sunset	1442/0521
M6.7	28 Aug	1619	3078	After sunrise	
M4.6	28 Aug	1832	3078	After sunrise	
M3.3	29 Aug	0338	3088	Before sunset	1445/0518
M8.6	29 Aug	1108	3088	Before sunrise	
M2.5	29 Aug	1456	3088	After sunrise	
M4.7	29 Aug	1857	3088	After sunrise	
M1.5	30 Aug	0213	3088	Before sunset	1447/0515
M2.1	30 Aug	1929	3088	After sunrise	

8. Instrumentation

A map shows the locations and geographic and geomagnetic coordinates of Anchorage Radio Observatory (ARO), Coho Radio Observatory (CRO) and HAARP Radio Observatory (HRO) (figure 16).

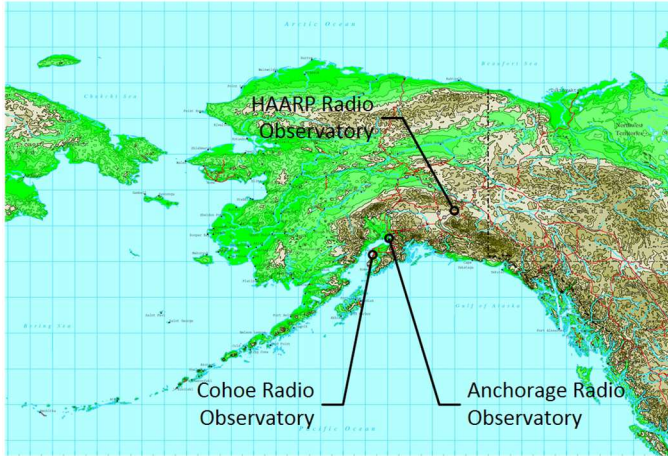


Figure 16 ~ Locations of the three observatories:

- ARO:** 22 m AMSL elevation
 61° 11' 57.70" N, 149° 57' 23.62" W geographic
 61.72° N, 94.41° W geomagnetic (2022)
- CRO:** 22 m AMSL elevation
 60° 22' 5.34" N, 151° 18' 55.74" W geographic
 60.71° N, 95.15° W geomagnetic (2022)
- HRO:** 562 m AMSL elevation
 62° 23' 21.00" N, 145° 8' 15.18" W geographic
 63.62° N, 90.61° W geomagnetic (2022)

Underlying map source: USGS

The instrumentation at each of the three observatories is described in terms of block diagrams (figure 17, 18 and 19). Shown here mostly are the systems and subsystems used to produce the above-described plots. Each observatory has additional antennas, receivers and instruments not shown; for example, seismometers, weather stations and infrasound detectors. The spectra displayed in sections 2 and 3 were produced by identical installations of Callisto instruments and an LWA Antenna at Cohoe Radio Observatory and HAARP Radio Observatory. These systems supply data during daylight hours to the e-CALLISTO Solar Radio Spectrometer Network [{e-CALLISTO}](#).

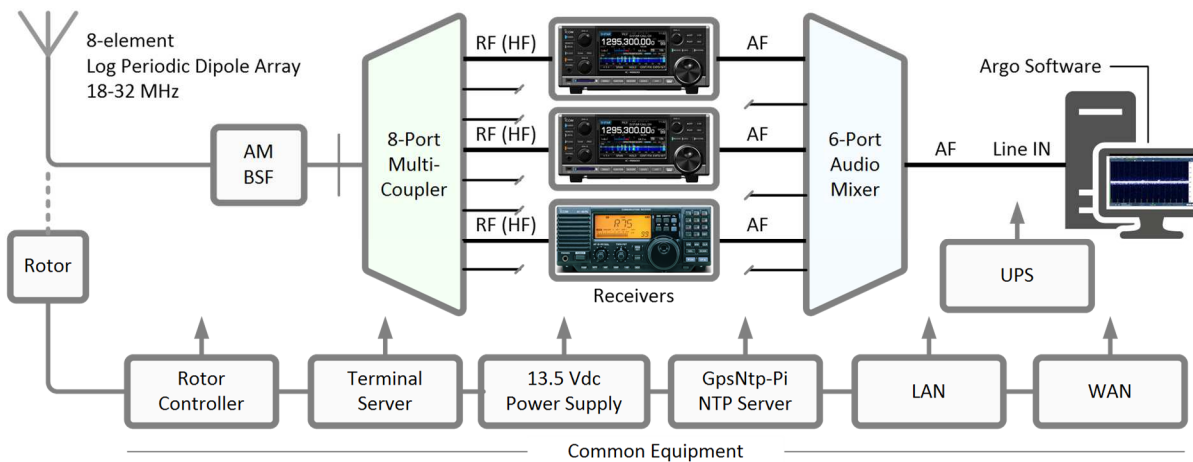


Figure 17.a ~ Anchorage Radio Observatory block diagram. Only the receiver and antenna systems used for this article are shown. The infrastructure along the bottom is shared by the various receiver and antenna systems and instruments.

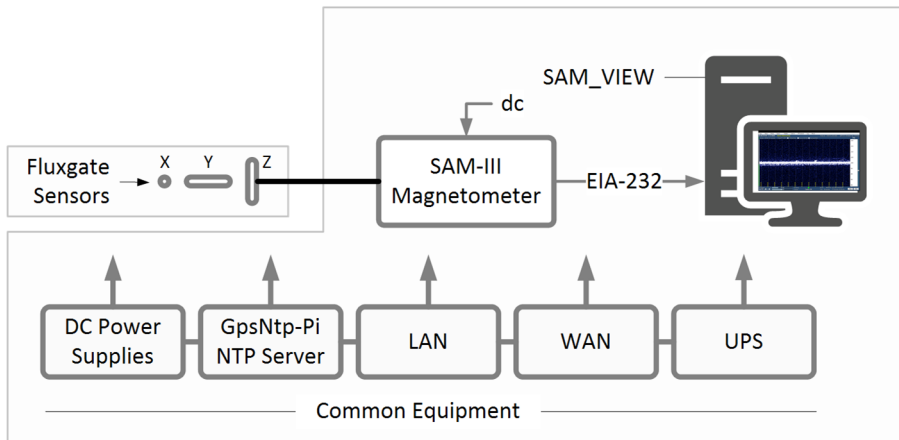


Figure 17.b ~ SAM-III magnetometer at Anchorage Radio Observatory. The SAM_VIEW software collects serial data from the SAM-III Controller at a 1/10 Hz rate. The three magnetic sensors are buried about 1 m below the ground surface to reduce the effects of daily temperature variations on sensor operation.

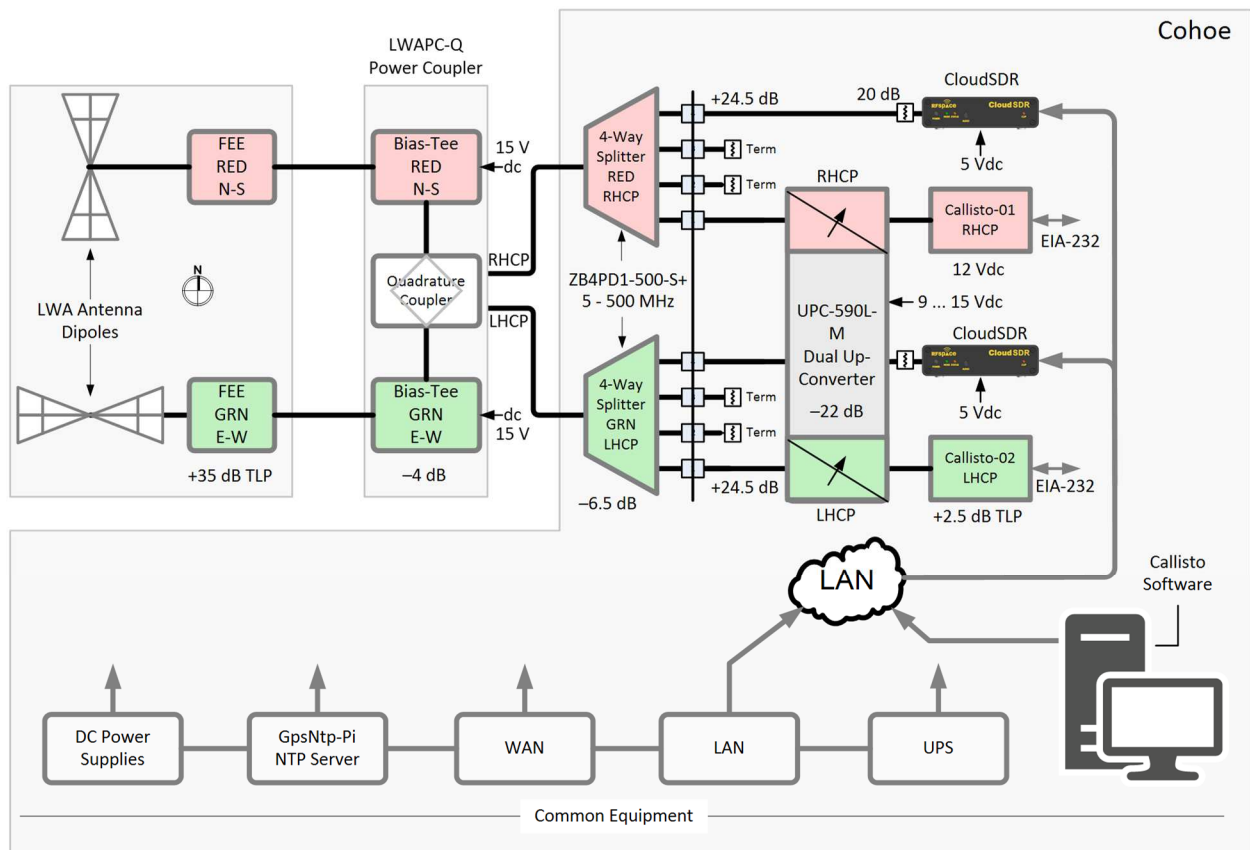


Figure 18.a ~ Cohoe Radio Observatory block diagram. The infrastructure along the bottom is shared by the various receiver and antenna systems and instruments.

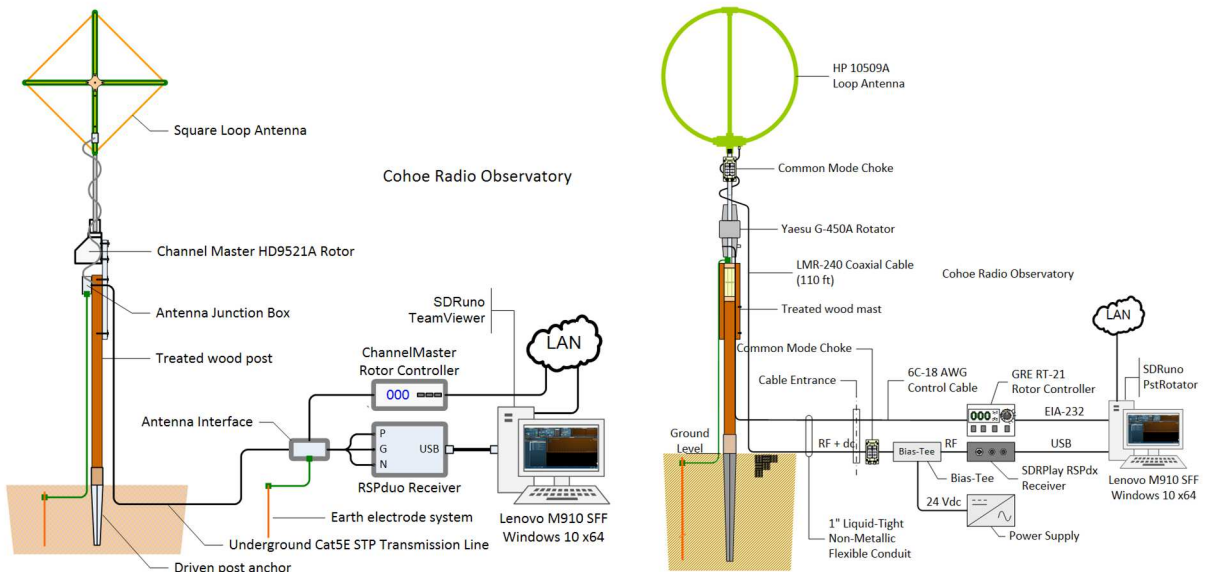


Figure 18.b ~ Two loop antennas and associated software defined radio (SDR) receivers are used at Cohoe Radio Observatory. This caption only briefly describes the setups; the loop antennas and receivers are more fully described at {ReevelF}. **Left:** One loop is a shop-built square loop antenna with 1.2 m diagonal on a modified Channel Master rotator for web control. This antenna is connected to an SDRPlay RSPduo receiver through the balanced interface and CAT5E cable. The receiver was tuned to 21.4 kHz during August 2022. **Right:** The other loop is a 1.1 m diameter refurbished HP circular active loop with an antenna-mounted, shop-built preamplifier. The antenna is mounted on a Yaesu G450-A rotator controlled by a Green Heron Engineering RT-21 controller with web control through the PstRotatorAz software application. This antenna is connected through a shop-built Loop Power Coupler and two common mode chokes to an SDRPlay RSPdx SDR receiver, which was tuned to 60 kHz during August 2022.

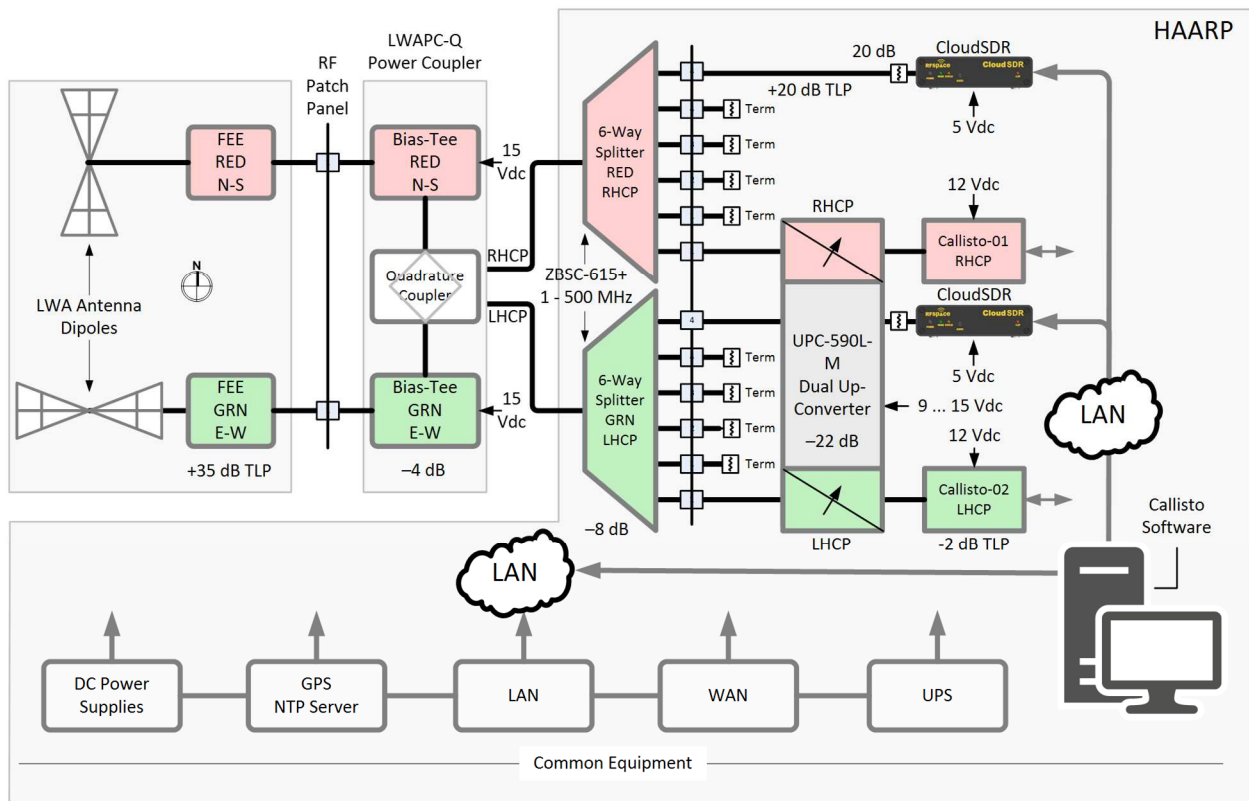


Figure 19 ~ HAARP Radio Observatory block diagram is almost identical to Coho. The Callisto instruments were the primary devices used during August. The SDR receivers shown in addition to the Callisto instruments are used to support HAARP experiments and radio propagation studies.

9. References & Further Reading

- {Callisto} <http://soleil.i4ds.ch/solarradio/callistoQuicklooks/>
- {e-CALLISTO} <https://e-callisto.org/>
- {Geomag} <https://reeve.com/Documents/SAM/GeomagnetismTutorial.pdf>
- {ReeveAurora} https://reeve.com/Documents/Articles%20Papers/Reeve_AuroraRadioObsrv.pdf
- {ReeveLF} https://reeve.com/Documents/Articles%20Papers/Reeve_SquareLoopAntenna1.2m.pdf and https://reeve.com/Documents/Articles%20Papers/Reeve_HP10509A_SSUpdate.pdf and https://reeve.com/Documents/Articles%20Papers/Reeve_VLF-LF-RFChoke.pdf and https://reeve.com/Documents/Articles%20Papers/Reeve_LoopPwrCplr.pdf
- {ReeveMeteor} https://reeve.com/Documents/Articles%20Papers/Reeve_MeteorRadioObsrv.pdf
- {ReeveSolar} <https://reeve.com/Solar/Solar.htm>
- {ReeveSFD} https://reeve.com/Documents/Articles%20Papers/Propagation%20Anomalies/Reeve_SuddenFreqDevConcepts_P1.pdf and https://reeve.com/Documents/Articles%20Papers/Propagation%20Anomalies/Reeve_SuddenFreqDevMeas_P2.pdf
- {SWPC} <https://www.swpc.noaa.gov/products/solar-cycle-progression>
- {Weekly} <ftp.swpc.noaa.gov/pub/warehouse/2022/WeeklyPDF>

Acknowledgement: Callisto FITS files, credit: FHNW Brugg/Windisch and IRSOL Locarno, Switzerland, {Callisto}

Document Information

Author: Whitham D. Reeve

Copyright: © 2022 W. Reeve

Revisions: 0.0 (Original draft started, 11 Sep 2022)
0.1 (Added Callisto observations, 17 Sep 2022)
0.2 (Formatted images, 18 Sep 2022)
0.3 (Added block diagrams and captions, 19 Sep 2022)
0.4 (Added loop antenna/receiver info, 20 Sep 2022)
0.5 (Finished 1st draft, 21 Sep 2022)
0.6 (Added ULF Waves plot, 22 Sep 2022)
0.7 (Distribution, 25 Sep 2022)
0.8 (Minor edits, 30 Sep 2022)
0.9 (Added Alaska map, 03 Oct 2022)

Word count: 2542

File size (bytes): 7164566